Holocene mercury accumulation calibrated by peat decomposition in a peat sequence from the Sanjiang Plain, northeast China

Chuanyu Gao, Shaoqing Zhang, Yunhui Li, Dongxue Han, Hanxiang Liu, Guoping Wang

PII: S1040-6182(18)30685-2

DOI: https://doi.org/10.1016/j.quaint.2019.01.020

Reference: JQI 7717

To appear in: *Quaternary International*

Received Date: 19 May 2018

Revised Date: 12 December 2018

Accepted Date: 20 January 2019

Please cite this article as: Gao, C., Zhang, S., Li, Y., Han, D., Liu, H., Wang, G., Holocene mercury accumulation calibrated by peat decomposition in a peat sequence from the Sanjiang Plain, northeast China, *Quaternary International* (2019), doi: https://doi.org/10.1016/j.quaint.2019.01.020.

Title page

Type of contribution: Research Paper

Title: Holocene mercury accumulation calibrated by peat decomposition in a peat sequence from the Sanjiang Plain, northeast China.

Names of authors:

Chuanyu Gao[1, 2], Shaoqing Zhang[1], Yunhui Li[1], Dongxue Han[1], Hanxiang Liu[1], and Guoping Wang[1 *]

Complete postal address(es) or affiliations:

1 Key Laboratory of Wetland Ecology and Environment, Northeast Institute of Geography and Agroecology, Chinese Academy of Sciences, Shengbei Street 4888, 130102, Changchun, China

2 ILÖK, Ecohydrology and Biogeochemistry Group, University of Münster, Heisenbergstr. 2, 48149 Münster, Germany

Corresponding author: Guoping Wang; Phone: +86-431-85542339 ; Fax: +86-431-85542298; E-mail: wangguoping@neigae.ac.cn

Abstract: Peatlands are ideal archives that are widely used to reconstruct historical Hg accumulation around the world. However, decomposition of peat soils leads to Hg enrichment or depletion in peat profiles. To evaluate the impact of peat decomposition on historical Hg accumulation records, a 7800-year peat sequence from the Shenjiadian peatland (SJD-2, Sanjiang Plain, northeast China) was selected in this study. Based on the degree of peat humification and a generalized additive model (GAM), Hg accumulation rates (Hg ARs) were reconstructed and calibrated from the middle Holocene onward. The results showed that the Hg concentrations in the SJD-2 peat profile ranged from 11.9 to 55.3 ng g^{-1} and that the Hg AR ranged from 0.4 to 7.0 μg m^{-2} yr^{-1}; these values for both parameters were lower than their corresponding values observed in other peatlands around the world. Peat decomposition led to Hg depletion in peat soils to some extent, and the GAM could be used to evaluate the impact of peat decomposition on historical Hg ARs in peat sequences based on the degree of peat humification and calibration of Hg ARs. Before the Industrial Revolution, anthropogenic Hg sources caused the calibrated Hg ARs in the SJD-2 peat profile to slightly increase around 1300 cal. yr BP. Similar to other regions around the world, the calibrated Hg AR on the Sanjiang Plain also obviously increased from 3 to 8 μg m^{-2} yr^{-1} after global Hg emissions began to increase during the Industrial Revolution.

Keywords: Mercury; Peat decomposition; Generalized additive model; Northeast China

1. Introduction

Mercury (Hg), which is an important trace element, was widely used in metallurgy and human activities several thousand years ago. Natural sources of Hg include volcanic activity, forest fires, natural weathering, and soil emissions, whereas anthropogenic sources of Hg include fossil-fuel combustion, industrial manufacturing, mining and smelting (Azoury et al., 2013; Pirrone et al., 2010). The raw material of mercury ores and other metal minerals present during ore smelting have caused large amounts of gaseous mercury to be released into the atmosphere (Mighall et al., 2002).

With the development of metal smelting, Hg produced by human activities continued to increase around the world from the Bronze Age to the Industrial Age (Drexler et al., 2016). Over large regions of the globe, human-related Hg emissions have increased relative to natural sources since the Industrial Revolution, in the middle of the 18th century (Elbaz-Poulichet et al., 2011; Mast et al., 2010). With the development of industry and mining, increases in anthropogenic Hg production became the major factor causing Hg accumulation rates (Hg ARs) in natural ecosystems to markedly increase after the Industrial Revolution (Corella et al., 2017; Farmer et al., 2009). Gaseous elemental Hg can be maintained in the atmosphere for approximately 1 year and can be widely transferred on a hemispheric scale (Martınez-Cortizas et al., 1999). Because of the atmospheric circulation and long retention time of Hg in atmosphere, large amounts of Hg produced from anthropogenic sources had exerted a serious influence on Hg deposition globally, and high Hg ARs since the Industrial Revolution have been widely reported in many regions around the world (Corella et al., 2017; Daga et al., 2016; Elbaz-Poulichet et al., 2011).

In China, the earliest mining or smelting activities can be traced back to the Xia Dynasty in 2100 BC-1700 BC. The Iron Age began nearly 700 years later in northeastern China than in the center of China, and the lifestyles of local residents began to be influenced by Chinese culture from central China during the Qin Dynasty (approximately 200 BC) (Xue et al., 1991). Historical Hg ARs increased in several regions around the world when iron tools became widely used for human activities (Li et al., 2016; Martinez Cortizas et al., 2016). However, few studies have focused on historical Hg ARs in northeast China; thus, the relationship between regional human activities and historical Hg accumulation in northeast China is still unclear. Historical variations in Hg ARs over the last several thousands of years can be observed using a number of types of environmental archives (e.g., lake sediments, peatlands) (Drexler et al., 2016; Mast et al., 2010). Similar to other ecosystems, peatlands are an important environmental archive that are widely distributed around the world (Yu et al., 2010). Due to the anaerobic environment of peatlands and their ability to receive dust via atmospheric deposition, trace elements are deposited and restored in peatlands (Martini et al., 2007). Thus, peatlands have been widely used to reconstruct the historical deposition fluxes of trace elements in previous studies (Bao et al., 2016; Bao et al., 2012; Ohlson et al., 2006).

In addition to Hg deposition, previous works have suggested that Hg concentrations in peatlands are also affected by the degree of peat decomposition (Biester et al., 2003; Zaccone et al., 2009). It is also difficult for most age-depth models to consider and modify the influence of peat decomposition on peat accumulation rates (Blaauw and Christen, 2011). Thus, peat decomposition means that the historical Hg ARs reconstructed based on peat accumulation rates and Hg concentrations may not directly reflect historical Hg deposition. To decrease the impact of peat decomposition on the results of Hg AR reconstruction, the C/N mass ratio has been successfully used to evaluate the degree of peat decomposition and to calibrate the reconstructed results of historical Hg ARs in previous studies (Biester et al., 2003). However, the mass ratio of C/N cannot be employed to evaluate the degree of peat decomposition based on the characteristics of organic matter and might affect the calibrated Hg ARs. Similar to the mass ratio of C/N, the degree of peat humification is influenced by the characteristics of organic matter and is widely used as another indicator to evaluate the degree of peat decomposition in peatlands (Biester et al., 2014). Nevertheless, few studies have focused on the calibration of historical Hg ARs through peat decomposition indicators other than the mass ratio of C/N.

In this study, we selected a ^{14}C-dated profile (SJD-2) (Zhang et al., 2014) from the Shenjiadian peatland (Sanjiang Plain, northeast China) for the determination of Hg concentrations and estimation of historical Hg ARs over the past 7800 years on the Sanjiang Plain, northeast China. The degree of peat humification and the mass ratio of C/N were selected as two indicators for evaluation of the degree of peat decomposition in the SJD-2 peat profile. Based on a generalized additive model (GAM), historical Hg ARs were calibrated based on selected peat decomposition indicators in this study. Combining the calibrated Hg ARs with regional potential natural or anthropogenic Hg sources, the historical Hg sources and Hg ARs of the Sanjiang Plain (northeast China) were revealed. Finally, this paper provides some data on Hg ARs and Hg concentrations in the peatlands of northeast China.

2. Materials and methods

2.1. Site and sampling

The SJD-2 peat profile was sampled in the Shenjiadian (N46°34′54″; E130°39′44″) peatland in Sanjiang Plain, Northeast China (Fig. 1). Detailed information about the Shenjiadian peatlands can be found in Zhang et al. (2014). The studied site is located in the valley zone between Zhangguangcai ridge and Wanda Mountain, which has an annual mean temperature of 2.4 °C and an annual mean precipitation of 550 mm. In March 2010, the SJD-2 core was collected by peat digging (Zhang et al., 2014). The profile was recovered to a depth of 195 cm and sliced into sections that were 1 cm thick. This profile comprises silt sediments below 160 cm and peat above this depth. Samples were freeze-dried (at -40 °C and a pressure of approximately 50 bar) for one week; they were then milled (using an agate mortar and pestle) and homogenized.

2.2. Hg analysis

For Hg analysis, we measured all samples in the upper 10 cm, one of every two samples between 11-90 cm, and one of every five samples below 90 cm. A total of 73 samples were analyzed in this study. Total Hg concentrations were determined in freeze-dried samples using a DMA-80 mercury analyzer (Milestone, Italy). One of every ten samples was analyzed in duplicate as a control, and two standard reference materials (M2 and M3) of the moss Pleurozium schreberi (Steinnes et al., 1997) were run within each set of samples. The quantification limit was 0.01 ng g^{-1} and the mean recoveries were 70% ± 2.1% and 93% ± 4.8%, respectively. The differences between duplicates ranged from 4% to 9%, with a mean value of 6.3%.

2.3. Bulk density, LOI, N, and degree of peat humification

To determine peat bulk density, peat cylinders were dried at 105 °C to a constant weight. The dry weight and known volume of the peat cylinders were used to calculate their bulk density. Loss on ignition (LOI) was determined by burning approximately 0.5 g of dry peat at 550 °C for 6 h, and the ash contents are the residual materials left after LOI analysis. The carbon (C) concentrations were calculated from LOI (i.e., multiplying the organic matter content by 0.5) (Lamarre et al., 2012). Total nitrogen (TN) was determined through H_2SO_4 - K_2SO_4 - $CuSO_4$ - Se digestion in a Continuous Flow Chemical Analyzer, and the mean recovery were 97 - 103%. The degree of peat humification was estimated by performing colorimetry on peat alkaline extracts (Chambers et al., 2011). Prior to peat humification analysis, the dry peat samples were milled to particle sizes that were smaller than 180 μm. A total of 0.125 g of each peat sample was treated with 8% NaOH solution (50 ml, 90 °C) for 1 h. Each mixture was filtered and transferred to a 100-ml flask that was then filled with pure water. Then, the solutions were diluted with equally pure water and measured using a UV-2500 visible spectrophotometer at a 540-nm wavelength. The absorbance values of the solutions were characterized by their degree of peat humification (Vorren et al., 2012).

2.4. Chronology

To establish an age-depth model, eight samples were prepared following the protocol described by Zhou et al. (Zhou et al., 2002), and they were measured by acceleration mass spectrometry (AMS) in the Xi'an Accelerator Mass Spectrometry laboratory (Zhang et al., 2014). Their radiocarbon ages were calibrated to calendar ages using the CALIB Rev.7.0.1 software (Stuiver and Reimer, 2006) (Table 1). The chronology of the sequence was calculated using the cubic-spline method based on the 8 calibrated calendar age values, and the results of the age-depth model and peat accumulation rates were shown in previous studies (Zhang et al., 2014; Zhang et al., 2017).

2.5. Generalized additive model

Generalized additive models (GAMs) are regression models where smoothing splines are used instead of linear coefficients for covariates (Hastie & Tibshirani, 1990). This approach has been found to be particularly effective at handling complex, non-linear behaviors associated with ecological and environmental research (Gao et al., 2014b; Pearce et al., 2011). The additive model, in the context of a concentration time series, can be written in the form (Hastie & Tibshirani, 1990):

$$\log(y_i) = \sum_{i=1}^{n} s_j(x_{ij})^2 + \varepsilon_i$$

where y_i is the Hg AR in the ith sample, $s_j(x_{ij})$ is the smoothing function of the ith value of covariate j, n is the total number of covariates, and ε_i is the ith residual with $var(\varepsilon_i) = \sigma^2$, which is assumed to be gamma distributed. Smoothing functions are developed through a combination of model selection and automatic smoothing parameter selection using penalized regression splines, which optimize the fit and attempt to minimize the number of dimensions in the model (Wood, 2011). The choice of the smoothing parameters is made through restricted maximum likelihood, and 95% confidence intervals are estimated using an unconditional Bayesian method (Wood, 2011). This analysis was conducted using the ‘gam’ modeling function in the R environment for statistical computing with the package ‘mgcv’ (Team, 2015).

3. Results

3.1. Total nitrogen, mass ratio of C/N and degree of peat humification

The total nitrogen (TN) content, mass ratio of C/N and degree of peat humification in the SJD-2 peat profile are shown in Fig. 2c-e. The concentrations of TN were low at the surface (0-12 cm) and bottom (171-205 cm) of the profile, which yielded TN concentrations ranging from 2.2-7.2 mg g^{-1} and 0.8–7.1 mg g^{-1}, respectively. Between 13 and 170 cm, the TN concentrations fluctuated between 15 and 25 mg g^{-1}. The variations in LOI were similar to those in TN, and the LOI values fluctuated approximately 60% in the middle of the peat profile (5 - 165 cm). At the bottom of the profile, LOI markedly decreased to close to 10%.

The carbon concentrations determined in this study were calculated from LOI. Based on carbon concentrations and TN concentrations, the mass ratios of C/N were calculated and are shown in Fig. 2e. In the SJD-2 peat profile, the mass ratio of C/N ranged from 10 to 30, and low mass ratios of C/N were found in the upper layers. The mass ratio of C/N was approximately 25 in the bottom layers (lower than 100 cm), which was slightly higher than that in the upper layers, of approximately 20. The degree of humification exhibited similar variation trends to the mass ratio of C/N. The degree of humification was also low (i.e., lower than 15%) in the upper layers and increased with increasing depth. The highest value (55.9%) was found at a depth of 97-98 cm (Fig. 2f); then, the degree of humification decreased with increasing depth.

3.2. Hg concentrations and accumulation rates

The average concentration of Hg was 25.1±10.3 ng g^{-1}. The maximum concentration existed in the surface layers (i.e., the ca. 3 cm layer; 55.3 ng g^{-1}), and the minimum value appeared at ca. 50 cm (11.9 ng g^{-1}) (Fig. 3). Hg concentrations sharply decreased in the surface peat layers, and the Hg concentrations in the deeper peat layers (ca. 20 cm) were lower than 20 ng g^{-1}. As the depth of the peat layers increased from 10 to 80 cm, the Hg concentration increased from 10 to 20 ng g^{-1}. From 80 cm to the bottom, the Hg concentration showed slight fluctuations between 20 and 30 ng g^{-1}.

The peat accumulation rates in SJD-2 were calculated based on the age-depth model and dry bulk density (Fig. 2a). The Hg AR ranged from 0.5 to 7.0 μg m^{-2} yr^{-1}, with an average value of 2.2 ± 1.4 μg m^{-2} yr^{-1}. From the surface layers to 15 cm, the Hg AR decreased from 7.0 to 2.0 μg m^{-2} yr^{-1}. Between 15 and 80 cm, the Hg ARs were low (1.0 - 2.0 μg m^{-2} yr^{-1}) and exhibited no obvious fluctuations. An obvious peak of the Hg AR appeared approximately 95 cm, and the highest Hg AR was 6.8 μg m^{-2} yr^{-1}, which occurred at 94 cm. From 100 cm to the bottom, the Hg ARs fluctuated and were slightly higher than those in the middle of the peat profile (15 – 80 cm).

4. Discussion

4.1. Mercury concentrations and accumulation rates

The range of mercury concentrations in the SJD-2 peat profile (11.9 – 55.3 ng g^{-1}) was lower than those reported for other peatlands in nearby regions or at similar latitudes. For example, in the ombrotrophic peatland along the nearby Hongqi River in the Small Hinggan Mountains in northeast China (west of the Sanjiang Plain), the maximum recorded mercury concentration was 574.4 ng g^{-1}, and a major increase in the mercury concentration occurred from 9 cm to the surface, with an average mercury concentration of 111.3 ± 64.7 ng g^{-1} in deeper soils (Tang et al., 2012). In the middle of China (i.e., the Dajiuhu peatland), the Hg concentrations in surface peat soils range from 100-595 ng g^{-1} (Li et al., 2016) (Table 2), which is much higher than those in the SJD-2 peat profile in northeast China. The Hg concentrations in the SJD-2 peat profile were also lower than those in other peatlands around the world. In the surface layers of peat soils that accumulated after 1750 AD in particular, Hg concentrations are obviously increased around the world, to values of even higher than 100 ng g^{-1} (Allan et al., 2013). Based on these Hg concentrations, the ecological risk of Hg pollution in the SJD-2 peat profile is much lower in other peatlands around the world.

The elements that accumulate at the bottoms of peat profiles can be regarded as being influenced by few anthropogenic factors and can be used to determine the historical accumulation rates of natural elements (Daga et al., 2016; Gao et al., 2014a). In the SJD-2 peat profile, lower Hg ARs were found in the bottom layers of peat soils that accumulated before 2000 cal. yr BP (ranging from 0.4 to 4.4 μg m^{-2} y^{-1}) (Table 2). The low Hg ARs in the SJD-2 peat profile were similar to those reported from other sites before 1500 AD, such as the Pyenean (Europe) and Belgium (Europe) sites, where the Hg ARs were 1.5 – 2.5 and 1.3 – 2.4 μg m^{-2} yr^{-1}, respectively (Enrico et al., 2017). A natural Hg AR of approximately 1 μg m^{-2} yr^{-1} has been reported in peatland in Greenland (Europe) from before 1750 AD (Pérez-Rodríguez et al., 2018), and the Hg AR ranges from 1.0 – 1.4 μg m^{-2} yr^{-1} in Peru (South America) (Beal et al., 2014). The natural Hg ARs measured in the SJD-2 peat profile were higher than those as these sites. However, the natural Hg ARs in the Dajiuhu peatland (before 3000 cal. yr BP), which is located in the middle of China, range from 0.5 to 12 μg m^{-2} yr^{-1} and are higher than those in the SJD-2 peat profile (Li et al., 2016). In addition, the Hg ARs in the SJD-2 peat profile were also much lower than those observed in several sites in France (Europe) and Patagonia (South America), where the Hg ARs were more than 10 μg m^{-2} yr^{-1} before the Industrial Age (Daga et al., 2016; Elbaz-Poulichet et al., 2011). The one of the important potential factors is that the natural Hg sources (e.g., forest fires, natural weathering) may major influenced by climate characteristics and the location of studied regions. The similar latitude and climate characteristics in northeast China with other selected regions around the world cause the major Hg natural sources in these regions are similar, while, obvious different with middle and southern regions of China. Overall, the Hg ARs in northeast China were lower than those in the middle and southern regions of China and were similar to the average Hg ARs around the world when the major sources of Hg were natural sources.

Comparing the Hg ARs during different periods in the SJD-2 peat profile reveals that the anthropogenic sources of Hg began to influence the Hg ARs on the Sanjiang Plain around 2000 cal. yr BP, when the Iron Age started in northeast China (Tarasov et al., 2006). After 2000 cal. yr BP, the Hg ARs on the Sanjiang Plain increased from 1.0 to 7.0 μg m^{-2} yr^{-1}. The Hg AR in the SJD-2 peat profile recorded during the Industrial Revolution was approximately 7 μg m^{-2} yr^{-1}, and the maximum Hg AR occurred around 100 cal. yr BP, which was far lower than those observed in other sites around the world (Table 2). The maximum Hg AR in the SJD-2 peat profile occurred in the 1800s A.D., together with high global Hg production during the Industrial Age. However, in recent years, the Hg AR decreased to 6.0 μg m^{-2} yr^{-1} and exhibited trends that were slightly different than the historical Hg AR variation trends observed at other sites during this period. In South America, Hg ARs range from 3.4 – 5.0 μg m^{-2} yr^{-1} in lake sediments in Peru corresponding to the time at which anthropogenic Hg began to influence Hg accumulation (post-1800 A.D.); Hg ARs in Patagonia range from 10 to 26 μg m^{-2} yr^{-1} during this period (Hermanns & Biester, 2013; Daga et al., 2016). In addition to these two sites, the Hg ARs at most sites are higher than 10 μg

m^{-2} yr^{-1} or even higher than 100 μg m^{-2} yr^{-1}, which are both values that are obviously higher than the Hg ARs in the SJD-2 peat profile from northeast China (Table 2). Because there are more than 1000 kilometers between the Sanjiang Plain and the middle of China, which is the cultural and industrial center of China, the development of the economy and industry on the Sanjiang Plain occurred much more slowly than in other regions in China (Li and Yuan, 1996). A few local anthropogenic Hg sources around the Sanjiang Plain are responsible for most of the anthropogenic Hg in the SJD-2 peat profile, while additional Hg from other regions arrives through atmospheric transmission. Thus, Hg ARs in the SJD-2 peat profile started to increase together when global Hg production started to increase. Both natural and anthropogenic Hg AR (especially anthropogenic Hg AR) in the SJD-2 peat profile were lower than in other regions. The low Hg ARs and low Hg concentrations in the SJD-2 peat profile cause the ecological risk of Hg pollution in the SJD-2 peat profile to be much lower than those observed in other peatlands around the world.

4.2. Geochemical characteristics of peat soils in the SJD-2 peat profile

To determine the basic geochemical characteristics and decomposition conditions of peat soils in the SJD-2 peat profile, bulk density, LOI, and TN were selected to reveal basic geochemical characteristics, while the mass ratio of C/N and the degree of peat humification were selected to evaluate decomposition conditions in this study. The scatter plot and correlation coefficients between these five indicators were plotted with the ‘chart.Correlation’ function in the R environment with the ‘PerformanceAnalytics’ package (Peterson and Carl, 2014) and are shown in Fig. 3.

Geochemical indicators, such as LOI/ash content, can be used to distinguish between minerotrophic and ombrotrophic peatlands. LOI in the SJD-2 peat profile ranged from 6% to 85%, with an average value of approximately 66%. The ash content is the residual material that remains after LOI analysis; the average ash content of these samples was approximately 34%. The high ash content in the peat clearly identified it as being minerotrophic because ombrotrophic peat usually contains much lower ash contents (5-20%) (Shotyk, 1996). Thus, the SJD-2 peatland could be identified as a minerotrophic peatland. The bulk density values of most samples were approximately 0.2 g/cm^3. In addition, in a few bottom samples, the bulk density ranged from 0.5 to 1.0 g/cm^3 (Fig. 2). With an increasing bulk density, LOI, TN and the degree of peat humification all decreased. In contrast to these three indicators, the mass ratio of C/N decreased when the bulk density increased from 0.1 to 0.3 g/cm^3, after which it increased markedly. LOI was found to be highly positively correlated with TN and the degree of peat humification and negatively correlated with bulk density (Fig. 3). However, there was no significant difference between LOI and the mass ratio of C/N. The mass ratio of C/N was only significantly different than TN, and there was a weak negative correlation between TN and the mass ratio of C/N (-0.32, $P<0.01$). Similar to LOI, the degree of peat humification was also highly positively correlated with TN and negatively correlated with bulk density.

The degree of peat humification and the mass ratio of C/N are widely used to evaluate peat decomposition in peat soils (Biester et al., 2014; Broder et al., 2012). The mass ratio of C/N can also be used to evaluate carbon loss in peatlands, as a low mass ratio of C/N reflects more carbon loss in a peatland (Biester et al., 2003). In the SJD-2 peat profile, there is no significant difference between the degree of peat humification and the mass ratio of C/N. When the mass ratio of C/N decreased from 27 to 22, the degree of peat humification increased from 40% to 45%. In addition, the degree of peat humification fluctuated around 45% when the mass ratio of C/N decreased from 22 to 18. With more carbon loss occurring in other peat layers, the mass ratio of C/N was lower than 18, and the degree of peat humification also decreased obviously. With an increasing degree of peat decomposition (reflecting more carbon loss), the variation of the degree of peat humification (which first increased and then decreased) indicated that the relationship between peat decomposition and the degree of peat humification was not directly linear and was similar to the relationship between Hg and peat decomposition. In Hg accumulation, carbon loss in peat layers leads to more Hg accumulation in peat soils, and Hg ARs can be calibrated by the mass ratio of C/N (Biester et al., 2003). Hg may also be lost with a high degree of carbon loss in peat layers, and the mass ratio of C/N may not be suitable for calibrating Hg ARs in this type of peat sequence. A low degree of carbon loss causes the degree of peat humification to increase, and an opposite trend appears between a high degree of carbon loss and the degree of peat humification. Because of the similar trends of Hg and the degree of peat humification during peat decomposition, the degree of peat humification may act as a better indicator for calibrating Hg ARs in peat profile.

Because different climate characteristics lead to different degrees of peat decomposition in peat sequences, several previous studies have reconstructed historical climate change based on the degree of peat humification, which can be regarded as an indirect proxy (Vorren et al., 2012; Wang et al., 2010). Some results have shown that a warm and wet climate may result in a low degree of peat humification (Ma et al., 2009), whereas other studies have obtained opposite results (Wang et al., 2010). Based on the relationship between the degree of peat humification and peat decomposition previously discussed, we can hypothesize an explanation for the opposite results obtained in previous studies. Warm and wet climate characteristics could accelerate peat decomposition and increase the degree of peat humification; however, high peat decomposition can lead to more carbon loss and decrease the degree of peat humification in peat profiles. The different stages of peat decomposition may lead to different results between different peat profiles. Because the degree of peat humification increased and then decreased with a decrease in the mass ratio of C/N in the SJD-2 peat profile, the degree of carbon loss in the SJD-2 peat profile could not be interpreted based on the degree of peat humification, and the degree of peat humification could not be employed to reconstruct historical regional climate characteristics directly. Thus, the degree of peat humification in the SJD-2 peat profile could be only used to evaluate the degree of peat humification in the peat profile and to calibrate Hg ARs in the peat profile in this study.

4.3. Influence of peat decomposition on accumulated Hg

The ratio of C/N and the degree of humification are two indicators that are widely used to evaluate peat decomposition (Biester et al., 2014; Broder et al., 2012).

The above discussion indicates that there is a non-linear correlation between the mass ratio of C/N and the degree of peat humification in the SJD-2 peat profile and that these two indicators can be used to reflect the degree of peat decomposition in peatlands under different conditions. Thus, both of these indicators were selected for the GAMs. In addition, based on the Akaike information criterion (AIC) test, the final models were obtained using the model based on these parameters showing the lowest AIC value. The final model, which explained 69.3% of the observed deviance, can be written as follows:

$$\log(\text{Hg AR}) = s(\text{time}) + s(\text{degree of humification})$$

No other refinements resulted in any significant improvement to the models, and the results obtained with the GAM are shown in Fig. 4. Time ($F=8.16$, $P<0.001$) and the degree of humification ($F=3.94$, $P<0.05$) were found to have significant effects on the Hg AR. Similar to the hypothesis that the degree of peat humification is better than mass ratio of C/N for calibrating Hg ARs, the GAM showed the same results and divided the impact of peat decomposition on Hg ARs. The relationships of the Hg AR with peat decomposition and accumulation time are shown in Fig. 4a. With an increasing degree of peat humification, the impact of peat decomposition on Hg ARs was negative, and a high degree of peat humification, together with increased peat decomposition, caused some Hg loss in peat soils and decreased the Hg AR. In contrast, when the degree of peat humification increased from 30% to 50%, there was no clearly decreasing trend of Hg, and the Hg ARs were not influenced by peat decomposition when the degree of peat humification was lower than 30%. With an increasing degree of peat decomposition, the negative impact on Hg ARs meant that Hg was lost along with the total mass loss when the degree of humification increased from 10% to 30%, which indicated that Hg concentrations in peatland may not be influenced by peat decomposition. However, when the degree of peat humification increased from 30% to 60%, the effect on total Hg was stable; thus, Hg concentrations may increase with the total loss of peat mass.

To decrease the influence of peat decomposition on Hg AR, we predicted historical Hg ARs with the same degree of humification using the GAM. Compared with the original degree of peat humification, the degree of peat humification in the prediction model was the same in all peat layers and ranged from 10% to 60%; the results are shown in Fig. 5. When the degree of humification increased from 10% to 30%, Hg ARs decreased markedly. In contrast, there was no obvious decreasing trend in Hg ARs when the degree of humification increased from 30% to 60% before 4000 cal. yr BP. From 4000 cal. yr BP to the present, a more obvious decreasing trend of Hg ARs appeared as the predicted degree of humification increased from 10% to 30%, while no obvious decreasing trend of Hg ARs appeared when the degree of predicted humification increased from 30% to 60%. During this period, the degree of humification in the SJD-2 peat profile was higher than 30%. Similar to the previous discussion, peat decomposition could not have caused the loss of Hg in these layers, and the Hg ARs were mainly influenced by Hg deposition during this period.

In summary, increasing the degree of peat humification from 10% to 30% easily led to Hg loss in the peatland, and the GAM could be used to decrease the influence of peat decomposition on Hg ARs. Based on the GAM, the Hg ARs in peat profiles could be predicted and calibrated with the same degree of peat decomposition (i.e., the same degree of peat humification). Historical variations in the Hg ARs calibrated by the GAM with the same degree of peat decomposition could be regarded as the actual historical variations in Hg deposition fluxes.

4.4. Potential sources of Hg in the SJD-2 peat profile

Based on the GAM analysis, Hg is easily lost when the degree of peat humification increases from 10% to 30% and remains nearly stable when the degree of peat humification increases from 30% to 60%. Considering the range of the degree of peat humification in the SJD-2 peat profile, the Hg ARs predicted with the same degree of peat humification (30%, boundary between two conditions) were used to reflect regional historical deposition in this study. To evaluate the influence of potential Hg sources on Hg ARs in the SJD-2 profile, historical population data from Heilongjiang Province (Li & Yuan, 1996), data on temperature (average chain length of n-alkanes, ACL-ALK) and precipitation (proportion of aqueous biomarkers, Paq) indicators reconstructed based on biomarkers on the Sanjiang Plain (Zhang et al., 2017), temperature data reconstructed from pollen in Jingbo Lake (west of the Sanjiang Plain) (Li et al., 2011), wildfire frequency data reconstructed based on charcoal on the Sanjiang Plain (Zhang et al., 2015), and East Asian summer monsoon data reconstructed from stalagmite ^{18}O values in the Dongge cave (Wang et al., 2005) were used as indicators of historical climate and human activities, to evaluate the influence of potential Hg sources on Hg deposition in the SJD-2 peat profile (Fig. 6).

The first peak values of calibrated Hg ARs appeared from 3800 to 2700 cal. yr BP during the last 8000 years. Fires increase the concentrations of atmospheric carbonaceous particulate matter and atmospheric mercury (Crutzen et al., 1990; Lavous et al., 2000). Atmospheric mercury is influenced by fires and, thus, exhibits good relationships with both the frequency and intensity of fires (Wang et al., 2010; Cordeiro et al., 2002). Because intensive anthropogenic activities began to influence the Sanjiang Plain around 1200 cal. yr BP (Cong et al., 2016), the frequency of fires was mainly influenced by regional climate characteristics before 1200 cal. yr BP. Based on lipid biomarkers and grain-size records in SJD-2, the climate on the Sanjiang Plain was cold and wet from 6000 to 4000 cal. yr BP under the strong summer monsoon, before shifting to warmer and drier conditions after 4000 cal. yr BP (Zhang et al., 2017). The SJD-2 peat profile recorded a transformation from a shallow lake to peatland around 4000 cal. yr BP (Zhang et al., 2014; Zhang et al., 2017). Several periods with high frequencies of fires recorded in the Honghe peatland on the Sanjiang Plain occurred around 2700 and 800 cal. yr BP (Zhang et al., 2015). The high frequency of natural fires from 3800 yr to 2700 cal. yr BP may be the major reason that the Hg ARs increased to 2 μg m^{-2} yr^{-1} during this period.

The amount of Hg produced by human activities during the Iron Age was obviously greater than that produced during the Bronze Age, which led the Hg ARs to increase around the world during the Iron Age (Martínez Cortizas et al., 2013; Martinez Cortizas et al., 2016). The Iron Age began around 2200 cal. yr BP in northeast China, nearly 700 years after it began in the middle of China and Europe

(Tarasov et al., 2006). After 2200 cal. yr BP, the population around the Sanjiang Plain also started to increase (Li and Yuan, 1996), and the increasing human activities caused more Hg to accumulate in the natural ecosystem. The Hg AR on the Sanjiang Plain started to increase during the Iron Age, and an obvious peak appeared around 1300 cal. yr BP; the calibrated Hg AR increased to nearly 4 μg m^{-2} yr^{-1} during this period. The climate of the Sanjiang Plain was warm and dry around 1500 cal. yr BP, which caused fires to occur more easily during this period (Li et al., 2011). One famous war occurred on the Sanjiang Plain around 1288 yr BP, and the black carbon deposits and diagnostic ratios of polycyclic aromatic hydrocarbons (PAHs) in two wetlands in the eastern region of the Sanjiang Plain were also shown to have been obviously changed by regional human activities during this period (Cong et al., 2016). The increasing human activities around the Sanjiang Plain and the widespread use of iron tools in northeast China caused anthropogenic sources of Hg to increase after 2200 cal. yr BP. Thus, the increasing human activities and warm/dry climate characteristics around 1300 cal. yr BP caused the calibrated Hg ARs to be higher than those in surrounding periods (i.e., 4 μg m^{-2} yr^{-1}).

From 400 cal. yr BP to the present, the frequency of fires was nearly stable and slightly decreased, which means that the amount to Hg produced by natural fires was nearly stable. However, the calibrated Hg AR increased from 3 to 8 μg m^{-2} yr^{-1} during this period. Similar to the increase in global Hg production (Allan et al., 2013; Conaway et al., 2004), the increasing human activities in northeast China, together with the rise in Hg production from anthropogenic sources, caused the calibrated Hg AR in the SJD-2 peat profile to obviously increase. Furthermore, industrial factories began to be established in northeast China around the 1900s AD (50 BP), and gold mining activities in the Great Hinggan Mountains, which are located in the western region of the Sanjiang Plain, also started to produce gold in 1888 AD. Similar to other sites around the world, the increased production of Hg from regional anthropogenic sources caused the calibrated Hg AR to obviously increase over the past several hundred years. Thus, anthropogenic sources of Hg were the major sources responsible for increasing the calibrated Hg AR on the Sanjiang Plain from 400 cal. yr BP to the present.

In summary, the high frequency of natural fires from 3800 to 2700 cal. yr BP caused the historical calibrated Hg AR on the Sanjiang Plain to increase for the first time during the last 8000 cal. yr BP. With the regional population increasing and iron tools becoming more widely used by humans, human activities began to increase the calibrated Hg AR on the Sanjiang Plain around 2200 cal. yr BP. Together with the high frequency of natural fires, human activities caused an obvious peak period of the calibrated Hg AR around 1300 cal. yr BP. With increasing human activities, the anthropogenic sources of Hg became the major sources of Hg and caused the calibrated Hg AR to increase from 3 to 8 μg m^{-2} yr^{-1} after 400 cal. yr BP.

5. Conclusions

In this study, the historical Hg ARs in the SJD-2 peat profile from the Sanjiang Plain were reconstructed and calibrated based on the degree of peat humification using a GAM. The Hg concentrations in the SJD-2 peat profile ranged from 11.9 to 55.3 ng g^{-1}, and the Hg ARs ranged from 0.4 to 7.0 μg m^{-2} yr^{-1}; the values of both of these parameters were lower than their corresponding values in other peatlands around the world. Peat decomposition could have caused Hg loss in peat soils and influenced Hg accumulation. Based on the GAM, the Hg ARs modified by a unified degree of peat humification were closer to historical Hg deposition and could, thus, be used to reconstruct the Hg deposition history in a peatland. There were three periods in which the Hg ARs on the Sanjiang Plain were higher than those in adjacent periods (i.e., 3800 to 2700 cal. yr BP, around 1300 cal. yr BP and from 400 cal. yr BP to the present). Similar to other sites around the world, anthropogenic sources of Hg mainly increased during the Iron Age and gradually became the major sources of Hg in the most recent several hundred years. From 400 cal. yr BP to the present, the increase in anthropogenic sources of Hg caused the calibrated Hg AR on the Sanjiang Plain to increase from 3 to 8 μg m^{-2} yr^{-1}.

Acknowledgments

We thank Antonio Martinez Cortizas and Marta Pérez-Rodríguez for laboratory assistance and Hg analysis. The authors gratefully acknowledge the assistance of the Analysis and Test Center of Northeast Institute of Geography and Agroecology, Chinese Academy of Sciences. Financial support was provided by the National Natural Science Foundation of China (No. 41571191; 41701217) and the National Key Research and Development Project (No. 2016YFA0602301).

References

Allan, M., Le Roux, G., Sonke, J.E., Piotrowska, N., Streel, M., Fagel, N., 2013. Reconstructing historical atmospheric mercury deposition in Western Europe using: Misten peat bog cores, Belgium, Science of the Total Environment, 442, 290-301.

Azoury, S., Tronczynski, J., Chiffoleau, J.F., Cossa, D., Nakhle,K., Schmidt, S., Khalaf, G., 2013. Historical records of mercury, lead, and polycyclic aromatic hydrocarbons depositions in a dated sediment core from the Eastern Mediterranean, Environmental science & technology, 47(13), 7101-7109.

Bao, K., Shen, J., Wang, G., Sapkota, A., McLaughlin, N., 2016. Estimates of recent Hg pollution in Northeast China using peat profiles from Great Hinggan Mountains, Environmental Earth Sciences, 75(6).

Bao, K., Xing, W., Yu, X., Zhao, H., McLaughlin, N., Lu, X., Wang, G., 2012. Recent atmospheric dust deposition in an ombrotrophic peat bog in Great Hinggan Mountain, Northeast China, Science of the Total Environment, 431, 33-45.

Beal, S.A., Kelly, M.A., Stroup, J.S., Jackson, B.P., Lowell, T.V., Tapia, P.M., 2014. Natural and anthropogenic variations in atmospheric mercury deposition during the Holocene near Quelccaya Ice Cap, Peru, Global Biogeochemical Cycles, 28(4), 437-450.

Biester, H., Knorr, K.H., Schellekens, J., Basler, A., Hermanns, Y.M., 2014. Comparison of different methods to determine the degree of peat decomposition in peat bogs, Biogeosciences, 11(10), 2691-2707.

Biester, H., Martinez-Cortizas, A., Birkenstock, S., Kilian, R., 2003. Effect of peat decomposition and mass loss on historic mercury records in peat bogs from Patagonia, Environmental science & technology, 37(1), 32-39.

Blaauw, M., Christen, J.A., 2011. Flexible paleoclimate age-depth models using an autoregressive gamma process. Bayesian Analysis, 6(3), 457-474.

Broder, T., Blodau, C., Biester, H., Knorr, K.H., 2012. Peat decomposition records in three pristine ombrotrophic bogs in southern Patagonia, Biogeosciences, 9(4), 1479-1491.

Conaway, C.H., Watson, E.B., Flanders, J.R., Flegal, A.R., 2004. Mercury deposition in a tidal marsh of south San Francisco Bay downstream of the historic New Almaden mining district, California, Marine Chemistry, 90(1), 175-184.

Cong, J., Gao, C., Zhang, Y., Zhang, S., He, J., Wang, G., 2016. Dating the period when intensive anthropogenic activity began to influence the Sanjiang Plain, Northeast China, Scientific Reports, 6, 22153.

Corella, J.P., Valero-Garcés, B.L., Wang, F., Martínez-Cortizas, A., Cuevas, C. A., Saiz-Lopez, A., 2017. 700 years reconstruction of mercury and lead atmospheric deposition in the Pyrenees (NE Spain), Atmospheric Environment, 155, 97-107.

Daga, R., Ribeiro Guevara, S., Pavlin, M., Rizzo, A., Lojen, S., Vreca, P., Horvat, M., Arribere, M., 2016. Historical records of mercury in southern latitudes over 1600 years: Lake Futalaufquen, Northern Patagonia, Science of the Total Environment, 553, 541-550.

Drexler, J.Z., Alpers, C.N., Neymark, L.A., Paces, J.B., Taylor, H.E., Fuller, C.C., 2016. A millennial-scale record of Pb and Hg contamination in peatlands of the Sacramento-San Joaquin Delta of California, USA, Science of the Total Environment, 551-552, 738-751.

Elbaz-Poulichet, F., Dezileau, L., Freydier, R., Cossa, D., Sabatier, P., 2011. A 3500-year record of Hg and Pb contamination in a mediterranean sedimentary archive (the Pierre Blanche Lagoon, France), Environmental Science and Technology, 45(20), 8642-8647.

Enrico, M., Le Roux, G., Heimburger, L.E., Van Beek, P., Souhaut, M., Chmeleff, J., Sonke, J.E., 2017. Holocene Atmospheric Mercury Levels Reconstructed from

Peat Bog Mercury Stable Isotopes, Environmental Science and Technology, 51(11), 5899-5906.

Farmer, J.G., Anderson, P., Cloy, J.M., Graham, M.C., MacKenzie, A.B., Cook, G.T., 2009. Historical accumulation rates of mercury in four Scottish ombrotrophic peat bogs over the past 2000years, Science of the Total Environment, 407(21), 5578-5588.

Gao, C., Lin, Q., Bao, K., Zhao, H., Zhang, Z., Xing, W., Lu, X., Wang, G., 2014a. Historical variation and recent ecological risk of heavy metals in wetland sediments along Wusuli River, Northeast China, Environmental Earth Sciences, 72(11), 4345-4355.

Gao, C., Lin, Q., Zhang, S., He, J., Lu, X., Wang, G., 2014b. Historical trends of atmospheric black carbon on Sanjiang Plain as reconstructed from a 150-year peat record, Scientific Reports, 4, 5723.

Hastie, T.J., Tibshirani, R.J., 1990. Generalized additive models, CRC press.

Lamarre, A., Garneau, M., Asnong, H., 2012. Holocene paleohydrological reconstruction and carbon accumulation of a permafrost peatland using testate amoeba and macrofossil analyses, Kuujjuarapik, subarctic Québec, Canada, Review of Palaeobotany and Palynology, 186, 131-141.

Li, C., Wu, Y., Hou, X., 2011. Holocene vegetation and climate in Northeast China revealed from Jingbo Lake sediment, Quaternary International, 229(1-2), 67-73.

Li, Y., Ma, C., Zhu, C., Huang, R., Zheng, C., 2016. Historical anthropogenic contributions to mercury accumulation recorded by a peat core from Dajiuhu montane mire, central China, Environmental Pollution, 216, 332-339.

Li, S., Yuan, Z. Eds., 1996. Historical population in Heilongjiang Province. Heilongjiang Publishing Group. (Heilongjiang, China) (In Chinese).

Ma, C., Zhu, C., Zheng, C., Yin, Q., Zhao, Z., 2009. Climate changes in East China since the Late-glacial inferred from high-resolution mountain peat humification records, Science in China Series D: Earth Sciences, 52(1), 118-131.

Martínez Cortizas, A., López-Merino, L., Bindler, R., Mighall, T., Kylander, M., 2013. Atmospheric Pb pollution in N Iberia during the late Iron Age/Roman times reconstructed using the high-resolution record of La Molina mire (Asturias, Spain), Journal of Paleolimnology, 50(1), 71-86.

Martınez-Cortizas, A., Pontevedra-Pombal, X., Garcıa-Rodeja, E., Novoa-Munoz, J., Shotyk, W., 1999. Mercury in a Spanish peat bog: archive of climate change and atmospheric metal deposition, Science, 284(5416), 939-942.

Martinez Cortizas, A., Lopez-Merino, L., Bindler, R., Mighall, T., Kylander, M.E., 2016. Early atmospheric metal pollution provides evidence for Chalcolithic/Bronze Age mining and metallurgy in Southwestern Europe, Science of the Total Environment, 545-546, 398-406.

Martini, I.P., Cortizas, A.M., Chesworth, W., 2007. Peatlands: evolution and records of environmental and climate changes, Elsevier.

Mast, M.A., Manthorne, D.J., Roth, D.A., 2010. Historical deposition of mercury and selected trace elements to high-elevation National Parks in the Western U.S. inferred from lake-sediment cores, Atmospheric Environment, 44(21-22), 2577-2586.

Mighall, T.M., Abrahams, P.W., Grattan, J., Hayes, D., Timberlake, S., Forsyth, S., 2002. Geochemical evidence for atmospheric pollution derived from prehistoric copper mining at Copa Hill, Cwmystwyth, mid-Wales, UK, Science of the Total Environment, 292(1-2), 69-80.

Ohlson, M., Korbøl, A., Økland, R.H., 2006. The macroscopic charcoal record in forested boreal peatlands in southeast Norway, The Holocene, 16(5), 731-741.

Pérez-Rodríguez, M., Silva-Sánchez, N., Kylander, M.E., Bindler,R., Mighall, T.M., Schofield, J.E., Edwards, K.J., Martínez Cortizas, A., 2018. Industrial-era lead and mercury contamination in southern Greenland implicates North American sources, Science of the Total Environment, 613-614, 919-930.

Pearce, J.L., Beringer, J., Nicholls, N., Hyndman, R.J., Tapper, N.J., 2011. Quantifying the influence of local meteorology on air quality using generalized additive models, Atmospheric Environment, 45(6), 1328-1336.

Peterson, B.G., Carl, P., 2014. PerformanceAnalytics: Econometric tools for performance and risk analysis. R package version 1.4.3541.

Pirrone, N., Cinnirella, S., Feng, X., Finkelman, R., Friedli, H., Leaner, J., Mason, R., Mukherjee, A., Stracher, G., Streets, D., 2010. Global mercury emissions to the atmosphere from anthropogenic and natural sources, Atmospheric Chemistry and Physics, 10(13), 5951-5964.

Shotyk, W., 1996. Peat bog archives of atmospheric metal deposition: geochemical evaluation of peat profiles, natural variations in metal concentrations, and metal enrichment factors, Environmental Reviews, 4(2), 149-183.

Steinnes, E., Allen, R., Petersen, H., Rambæk, J., Varskog, P., 1997. Evidence of large scale heavy-metal contamination of natural surface soils in Norway from long-range atmospheric transport, Science of the Total Environment, 205(2-3), 255-266.

Stuiver, M., Reimer, P.J., 2006. Extended ^{14}C data base and revised CALIB 3.0 ^{14}C age calibration program. Radiocarbon 35, 215-230.

Tang, S., Huang, Z., Liu, J., Yang, Z., Lin, Q., 2012. Atmospheric mercury deposition recorded in an ombrotrophic peat core from Xiaoxing'an Mountain, Northeast China, Environmental Research, 118, 145-148.

Tarasov, P., Jin, G., Wagner, M., 2006. Mid-Holocene environmental and human dynamics in northeastern China reconstructed from pollen and archaeological data, Palaeogeography, Palaeoclimatology, Palaeoecology, 241(2), 284-300.

Team, R.C., 2015. R: a language and environment for statistical computing. Vienna, Austria; 2015, edited.

Vorren, K.D., Jensen, C.E., Nilssen, E., 2012. Climate changes during the last c. 7500 years as recorded by the degree of peat humification in the Lofoten region, Norway, Boreas, 41(1), 13-30.

Wang, H., Hong, Y., Lin, Q., Hong, B., Zhu, Y., Wang, Y., Xu, H., 2010. Response of humification degree to monsoon climate during the Holocene from the Hongyuan peat bog, eastern Tibetan Plateau, Palaeogeography, Palaeoclimatology, Palaeoecology, 286(3-4), 171-177.

Wang, Y., Cheng, H., Edwards, R.L., He, Y., Kong, X., An, Z., Wu, J., Kelly, M.J., Dykoski, C.A., Li, X., 2005. The Holocene Asian monsoon: links to solar changes and North Atlantic climate, Science, 308(5723), 854-857.

Wood, S.N., 2011. Fast stable restricted maximum likelihood and marginal likelihood estimation of semiparametric generalized linear models, Journal of the Royal Statistical Society: Series B (Statistical Methodology), 73(1), 3-36.

Yu, Z., Loisel, J., Brosseau, D.P., Beilman, D.W., Hunt, S.J., 2010. Global peatland dynamics since the Last Glacial Maximum, Geophysical Research Letters, 37(13), 1-5.

Zaccone, C., Santoro, A., Cocozza, C., Terzano, R., Shotyk, W., Miano, T.M., 2009. Comparison of Hg concentrations in ombrotrophic peat and corresponding humic acids, and implications for the use of bogs as archives of atmospheric Hg deposition, Geoderma, 148(3-4), 399-404.

Zhang, Y., Meyers, P.A., Gao, C., Liu, X., Wang, J., Wang, G., 2017. Holocene climate changes in northeastern China reconstructed from lipid biomarkers in a peat sequence from the Sanjiang Plain, Organic Geochemistry, 113, 105-114.

Zhang, Z., Xing, W., Lv, X., Wang, G., 2014. The grain-size depositional process in wetlands of the Sanjiang Plain and its links with the East Asian monsoon variations during the Holocene, Quaternary International, 349, 245-251.

Zhang, Z., Zhong, J., Lv, X., Tong, S., Wang, G., 2015. Climate, vegetation, and human influences on late-Holocene fire regimes in the Sanjiang plain, northeastern China, Palaeogeography, Palaeoclimatology, Palaeoecology, 438, 1-8.

Zhou, W., Lu, X., Wu, Z., Deng, L., Jull, A., Donahue, D., Beck, W., 2002. Peat record reflecting Holocene climatic change in the Zoigê Plateau and AMS radiocarbon dating, Chinese Science Bulletin, 47(1), 66-70.

Table 1. Radiocarbon dating by Accelerator Mass Spectrometry of peat core SJD-2. Depth shown from modern surface to bottom of peat sequence. Calibrated and conventional radiocarbon ages presented as years before present (yr BP, calibrated to 1950 A.D.). Calibrated dates indicated as median estimated age with 95% confidence limits. (Zhang et al., 2014).

Lab. Code	Depth(cm)	$\delta^{13}C$ (‰)		pMC (%)		^{14}C Age (yr BP)		
		$\delta^{13}C$	Error (1σ)	pMC	Error (1σ)	^{14}C Age	Error (1σ)	cal yr BP
XA7553	27	-37.78	0.51	93.39	0.28	550	24	541±20
XA7592	60	-38.64	0.48	87.34	0.27	1088	24	1004±52
XA7542	84	-30.36	0.37	84.2	0.27	1381	26	1308±31
XA7543	107	-24.56	0.4	81.2	0.32	1673	32	1577±58
XA7554	126	-22.74	0.56	81.16	0.24	1677	23	1577±49
XA7555	145	-34.31	0.48	80.62	0.3	1731	30	1635±75
XA7570	165	-30.14	0.36	64.34	0.21	3542	26	3857±46
XA7571	195	-48.99	1.03	41.93	0.47	6982	90	7816±158

Table 2. Hg concentrations and accumulation rates (AR) in peatland and lake sediments around the world. Based on the degree of local human activities, Hg was defined as natural Hg or anthropogenic Hg during different periods.

Location	Hg Concentrations ng/g	Hg AR μg/m^2.a	Year	Materials	Reference
Sanjiang Plain China, Asia	14-31; 12-55	0.4-4.4; 1.0-7.0	8ka to 2ka BP; Post 2ka BP	Peat	This study
Dajiuhu China, Asia	29-200; 100-595	0.5-12; 5-36	12ka to 3ka BP; Post 3ka BP	Peat	(Li et al., 2016)
Peru, South America	31-32; 68-70	1.0-1.4; 3.4-5.0	12ka to 3.5ka BP; Post 1800 AD	Lake	(Beal et al., 2014)
Patagonia, South America	27-47; 64-81	8-15; 10-26	1600 to 1850 AD; Post 1850 AD	Lake	(Daga et al., 2016)
Patagonia, South America	69-104; 186	30, 29	17ka to 5.4ka BP; Post 5.4ka BP	Lake	(Hermanns and Biester, 2013)
California, North America	50-150; 500-1200	180; 560-10000	Pre 1800 AD; Post 1800 AD	Tidal marsh	(Conaway et al., 2004)
Belgium, Europe	35-46; 29-1130	1.3-2.4; 8.3-137	Pre-1750AD; Post 1750AD	Peat	(Allan et al., 2013)
Spanish, Europe	22-100; 100-436	20-80; 80-440	Pre 1300 AD; Post 1300 AD	Peat	(Martınez-Cortizas et al., 1999)
Pyenean, Europe	38-218; 50-238	1.5-2.5; 6.0-40	10ka to 1500 AD; Post 1750 AD	Peat	(Enrico et al., 2017)
Greenland, Europe	9-60 47-297	<1 1-9.3	Pre 1750 AD; Post 1750 AD	Peat	(Pérez-Rodríguez et al., 2018)
France, Europe	20-129 36-577	3.3-115 41-462	Pre 1750 AD; Post 1750 AD	Lake	(Elbaz-Poulichet et al., 2011)

Figure Captions

Figure 1. Location of Shenjiadian (SJD-2) peatland.

Figure 2. Variation of bulk density, LOI, total nitrogen, the mass ratio of C/N, the degree of peat humification, Hg concentrations (Hg conc.), and Hg accumulation rates in the SJD-2 peat core.

Figure 3. Correlation coefficients and scatter plots of dry density, LOI, total nitrogen (TN), the mass ratio of C/N (C.N ratios), and the degree of peat humification (Humification). On top, the absolute value of the correlation plus the results of the test for an association between paired samples are indicated with stars.

Figure 4. Estimated smooth terms of Hg accumulation rates for the GAM. (a) The smooth function of calendar years. The y-axis represents historical deposition of Hg; (b) Smooth function of the degree of peat humification. The y-axis represents the impact of peat humification on Hg accumulation rates. The grey shadow is the 95% confidence interval.

Figure 5. Calibrated Hg accumulation rates based on peat decomposition proxies. a Historical calibrated Hg accumulation rates (ARs) with the same degree of peat humification (from 10 to 60%) predicted by the GAM; b historical variations in the degree of peat humification and the mass ratio of C/N in the SJD peat core; c historical variations in ash contents in the SJD-2 peat core.

Figure 6. Historical calibrated Hg accumulation rates in the SJD-2 peat profiles and their potential influencing factors. a Historical Hg accumulation rates (ARs) calibrated by the GAM, with the degree of peat humification defined as 30%; b, warm tree species in Jingbo Lakes, northeast China (Li et al., 2011); c, temperature (average chain length of n-alkanes, ACL-ALK) and precipitation (proportion of aqueous biomarkers, Paq) indicators in the SJD peatland reconstructed based on liquid biomarkers (Zhang et al., 2017); d, Regional fire frequency recalculated based on charcoal data in the Honghe peatland, north of the Sanjiang Plain (Zhang et al., 2015); e, historical intensity of the East Asia monsoon reconstructed from DG $\delta^{18}O$ data (Wang et al., 2005); f, historical population in Heilongjiang Province (summarized by Cong et al., 2016); g, Bronze Age, Iron Age, and Industrial Age in Europe, the center

of China and northeast China.

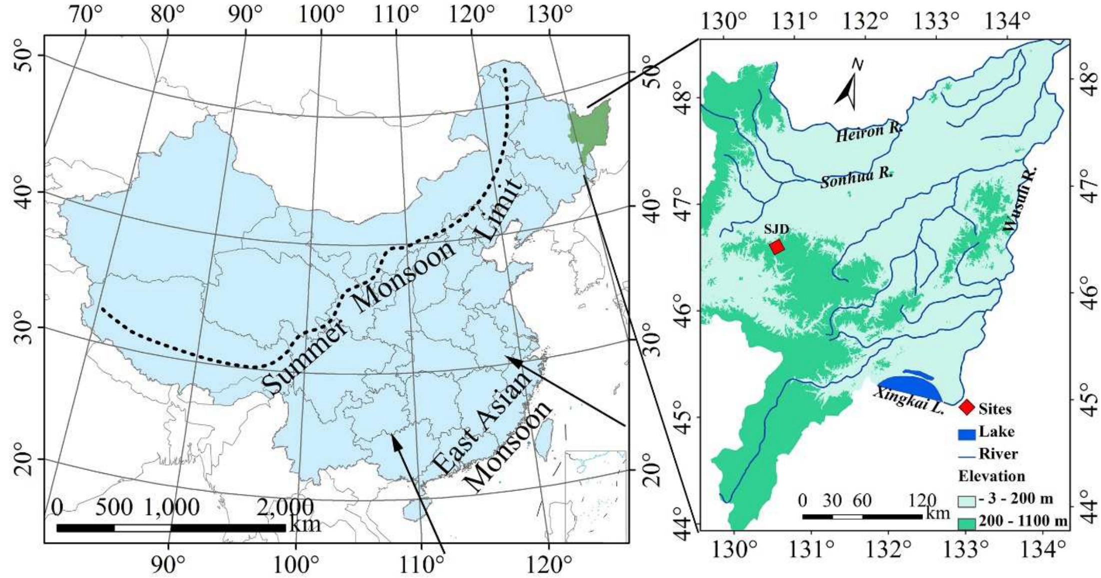

Figure 1

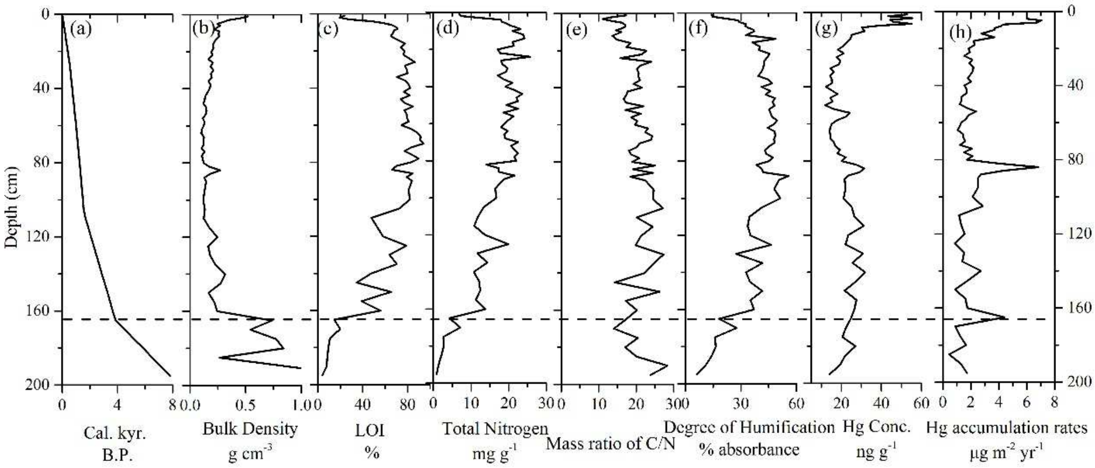
(a)
(b)
(c)
(d)
(e)
(f)
(g)
(h)
Depth (cm)
0
40
80
120
160
200
Cal. kyr. B.P.
0 4 8
Bulk Density g cm-3
0.0 0.5 1.0
LOI %
0 40 80
Total Nitrogen mg g-1
0 10 20 30
Mass ratio of C/N
0 10 20 30
Degree of Humification % absorbance
0 30 60
Hg Conc. ng g-1
0 20 40 60
Hg accumulation rates µg m-2 yr-1
0 2 4 6 8

Figure 2

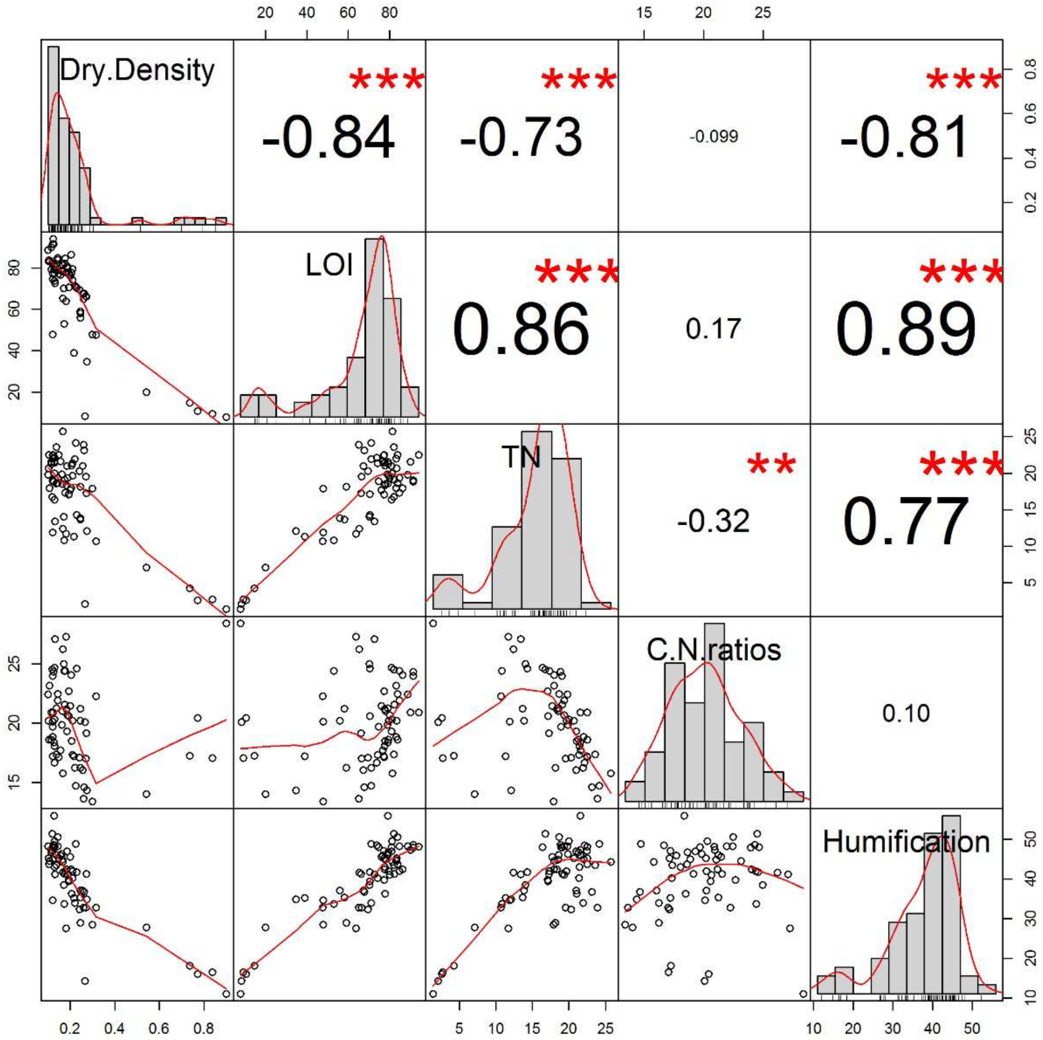
Dry.Density
LOI
TN
C.N.ratios
Humification
-0.84 ***
-0.73 ***
-0.099
-0.81 ***
0.86 ***
0.17
0.89 ***
-0.32 **
0.77 ***
0.10
20 40 60 80
15 20 25
0.2 0.4 0.6 0.8
5 10 15 20 25
10 20 30 40 50

Figure 3

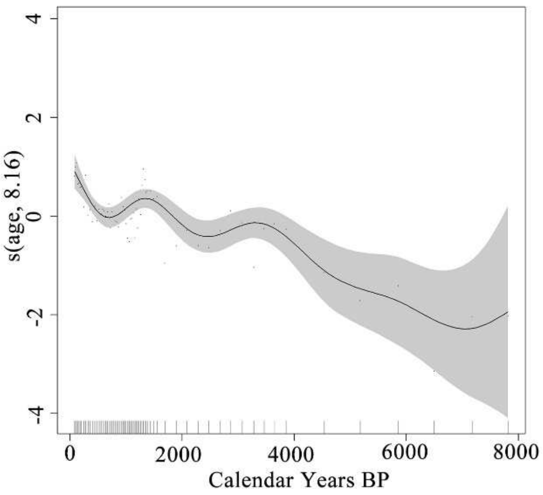
s(age, 8.16)
4
2
0
-2
-4
0
2000
4000
6000
8000
Calendar Years BP

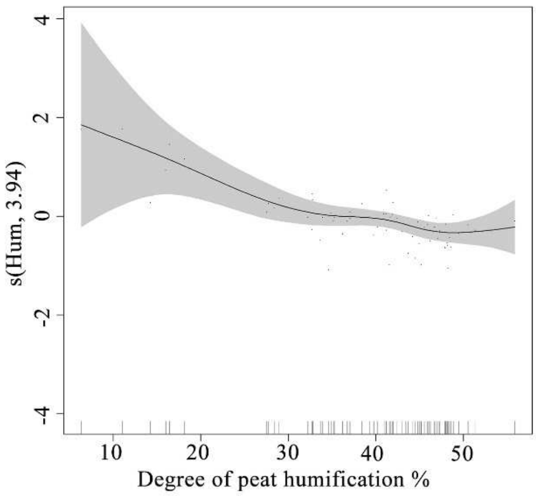
s(Hum, 3.94)
4
2
0
-2
-4
10
20
30
40
50
Degree of peat humification %

Figure 4

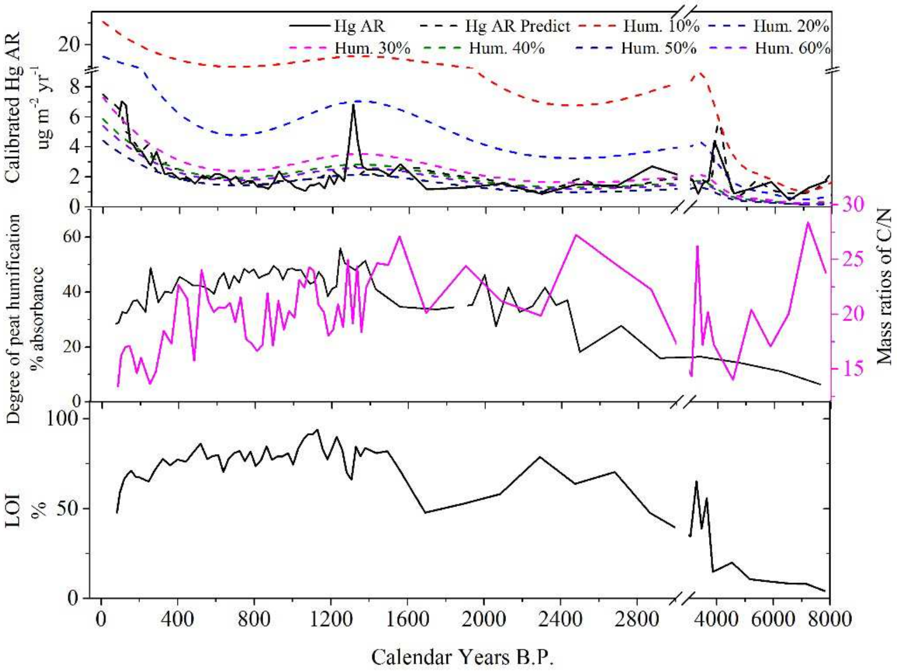
Hg AR
Hg AR Predict
Hum. 10%
Hum. 20%
Hum. 30%
Hum. 40%
Hum. 50%
Hum. 60%
Calibrated Hg AR
ug m-2 yr-1
20
8
6
4
2
0
Degree of peat humification
% absorbance
60
40
20
0
Mass ratios of C/N
30
25
20
15
LOI
%
100
50
0
0
400
800
1200
1600
2000
2400
2800
4000
6000
8000
Calendar Years B.P.

Figure 5

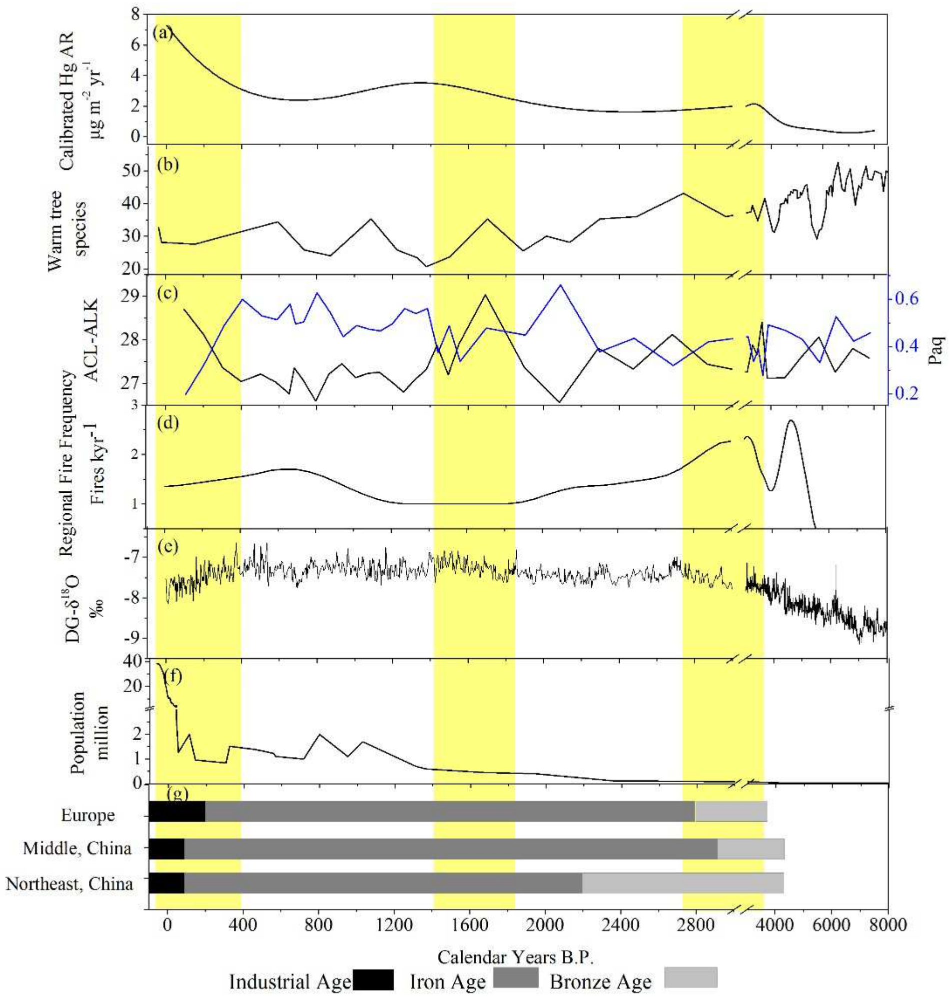
Calibrated Hg AR μg m-2 yr-1
(a)
8
6
4
2
0
Warm tree species
(b)
50
40
30
20
ACL-ALK
(c)
29
28
27
Paq
0.6
0.4
0.2
Regional Fire Frequency Fires kyr-1
(d)
3
2
1
DG-δ18O ‰
(e)
-7
-8
-9
Population million
(f)
40
20
2
1
0
(g)
Europe
Middle, China
Northeast, China
0
400
800
1200
1600
2000
2400
2800
4000
6000
8000
Calendar Years B.P.
Industrial Age
Iron Age
Bronze Age

Figure 6